

Surface-Directed Nanoepitaxy on a Surface with an Irregular Lattice

Elias Garratt and Babak Nikoobakht*

There remain many challenges to incorporating nanosystems in current device architectures, including spatially controlled positioning of active areas in nanosystems, electrically addressing nanosystem networks, and control over hierarchy of nanosystems. Many platforms have emerged to address these challenges including lithography and bottom-up fabrication.^[1,2] Currently, high-end devices such as computer processors can only be reliably fabricated using advanced lithography techniques, but due to their restrictively high cost such technologies may not find use in other branches of nanotechnology such as sensing and photonics sensing, photonics or integration of 1 and 2D nanostructures in electronic devices.^[3] As a result, in recent years bottom-up fabrication methods have been more refined to allow higher precision and control^[4] over registries of nanocrystals for their collective integration and low cost.^[5,6] However, most of these techniques often require transfer of nanostructures from source to target surfaces that are not suitable to deliver the required precision in hierarchy and function on a large scale.^[2,6] Surface-directed vapor–liquid–solid (SVLS) growth of nanocrystals^[7] has become known for its desirable characteristics, namely, precise and predictable positioning/orientation and elimination of postgrowth nanowire (NW) alignment.^[8–10] This approach exploits the surface crystal information of the substrate to laterally guide nanocrystals in predictable directions and has been demonstrated on a variety of materials including ZnO,^[7] GaAs,^[10] In₂O₃,^[11,12] GaN,^[13] Ge,^[11] Mg₂SiO₄,^[14] TiO₂,^[8] and ZnSe.^[15] The compatibility of the SVLS growth process with semiconductors and conventional optical photolithography is expected to lead to breakthroughs in transitioning nanosystems to complex 2 and 3D architectures and ultimately to practical applications.

Low dimensional nanosystems, such as NWs, provide more degrees of freedom in managing internal defects, lattice strain,^[16] and doping profile;^[17] however, their response to external stimuli remains unclear and underutilized. External stimuli could include surface impurities, surface lattice disorder, or foreign adlayers that could interface with a nanocrystal during their growth, assembly, or device duty cycles. To utilize these nanosystems for realization of scalable surface nanoengineering methods and reproducible architectures, we need to quantitatively assess and develop models on how nanocrystals respond to such external effects, e.g., structural evolution, defect propagation, and variation in nanocrystal function.

In this work, we present early results on a general approach for surface-directed nanocrystal epitaxy on a surface with an irregular lattice constant. We trace the growth behavior of a nanocrystal when it transits from a continuous lattice matched region to a discontinuous one to explore the tolerance of nanocrystals to defect formation when a sudden variation in lattice mismatch occurs. In this regard, nanoepitaxy is investigated on a surface that only contains patches of lattice matched areas in a background with surface lattice disorder. We use ZnO and GaN that have a slight lattice mismatch of 1.9% and form periodic arrays of surface disorders on GaN by scrambling the order of surface atoms using a tightly focused pulse of Ga ions. The threshold of failure in nanocrystal epitaxy is found to depend on the spacing between the patches and their total surface area. By adjusting this threshold, it is possible to scalably restrict nanocrystal growth, filter out single nanowires and partition nanowire heterojunctions into segments with different orientation or modulate their electronic structures. The proposed nanoepitaxy could also be considered as a model system to mimic how a laterally growing nanocrystal (nanowire) responds and interfaces with small islands of 2D inorganic membranes deposited on a mismatched background.

The SVLS lateral growth process is used as it allows the Au/semiconductor/substrate interface to advance on the substrate as the nanocrystal grows. This behavior offers a unique circumstance to use the underlying surface structure (that is deliberately placed on the nanocrystal growth path) to alter properties of specific parts of the nanocrystals on a large scale, a feature that cannot be realized in the traditional thin film growth or free-standing NW growth. High-resolution transmission electron microscopy (HRTEM) and cathodoluminescence (CL) microscopy are used to reveal the impact of such miniature surface alteration on the postgrowth structure of the nanocrystals including epitaxy, directionality, and variation in local properties of the formed heterojunctions.

Lattice surface disorder on GaN substrate at a controlled pitch is introduced using short-pulses of a focused Ga ion beam (FIB) ranging from 9 to 262 ions/pulse at 30 keV. Energetic ions colliding with surface crystal atoms cause damage by displacing those atoms, leaving surface vacancies. **Figure 1a** (right), schematically, shows the exposed unit cells of (0001) GaN lattice to 85 Ga ions within a 7 nm beam spot. Both the ion and displaced atom can then continue ricocheting into the crystal, causing more displacement and interstitials before eventually stopping. By fixing the length of each pulse of ions, we can control the number of ions introduced and their location within a 7 nm diameter spot, thereby controlling the location and amount of disorder to the substrate. In **Figure 1a** (left), ion line patterns were drawn onto the surface of the Ga-terminated (0001) GaN substrate at off-axis angles relative to the growth vectors of ZnO

Dr. E. Garratt, Dr. B. Nikoobakht
Materials Measurement Science Division
National Institute of Standards and Technology
Gaithersburg, MD 20899, USA
E-mail: babakn@nist.gov

DOI: 10.1002/admi.201500598



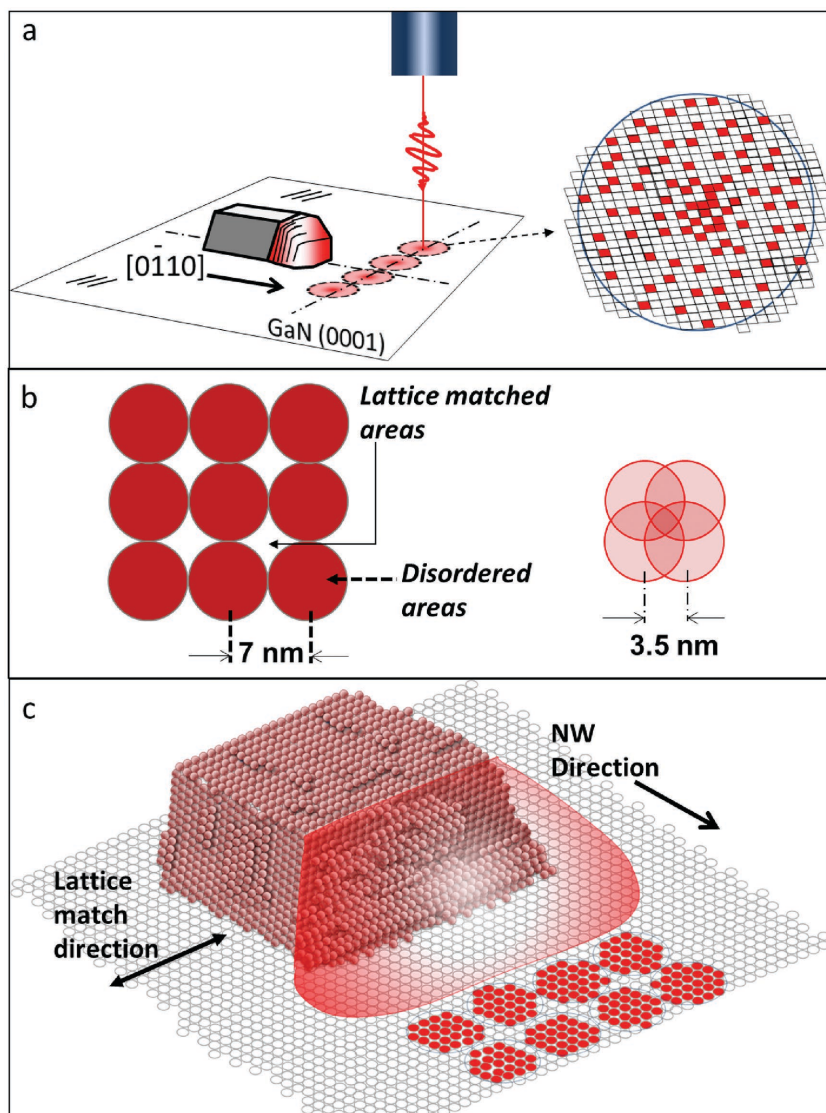


Figure 1. a) Methodology to introduce ordered patches within a disordered area (left), and distribution of ions within the beam spot knocks out lattice atoms and creates disorder (right). b) 7 nm ion beam spots are used to create disorder patterns with 7 or 3.5 nm pitch via changing the spot overlap from zero to 50%, respectively. c) A crawling NW encountering a pattern of disorder with a 7 nm pitch. The direction that the two crystals match and the NW growth direction are highlighted.

nanocrystals (i.e., GaN *m*-directions)^[8] to ensure the intersection of the nanocrystal growth vector with the disorder pattern. The short pulses of Ga ions on the GaN surface generated spot arrays with about 7 and 3.5 nm pitches when beam spots have a 0% and 50% overlap, respectively (Figure 1b).

As illustrated in Figure 1c, during the SVLS growth, thin nanocrystals sequentially form at the interface of the Au/nanocrystal. The width of the nanocrystal is defined by the diameter of the Au droplet and the preferred growth direction of the nanocrystal is the direction at which the two lattices match, namely, orthogonal to the NW direction.^[8] Based on previous HRTEM results, a 60 nm wide ZnO NW is expected to have a growth pitch of about 12 nm along its long axis.^[18]

The primary questions to answer are the extent to which miniscule changes on the GaN surface (Figure 1c, red patches) interfere and impact a lattice-matched heteroepitaxial nanosystem such as ZnO/GaN. For instance, how structural characteristics of each segment of the NW change as well as its extent of coupling with the previous and following sections of the nanocrystal.

Introducing spot arrays made from 9, 26, 85, and 262 Ga⁺ ions per spot with a 7 nm pitch (0% overlap) does not impact the nanocrystal growth. This behavior is shown in the scanning electron micrograph (SEM) image in Figure 2a and schematically in Figure 2b for the 85 ions/spot exposure. NWs pass over the disordered region along the GaN *m*-direction, i.e., $1\bar{1}00$. To better understand the degree of ion collision induced disorder within each spot, taking into account ion distribution within the beam, SRIM^[19] simulation was used. In the case of 85 ions/pulse simulations estimate an average displacement probability of 1.8 atoms/1 unit cell. Increasing the number of ions/pulse/spot to 262 results in an about 3.3-fold increase in the average number of displaced surface atoms translating to a displacement of 5.4 atoms/1 unit cells. As seen in Figure 2c,d, although the extent of damage in the lattice is increased three times, it still does not impede the passage of NWs or their directionality. We note that in the case of a 0% overlap, there is a considerable number of unexposed diamond-shaped regions on GaN between the beam spots (Figure 1b). Simple geometrical considerations indicate that this area is about 20% of the region that a 12 nm segment (of a 60 nm wide ZnO NW) crawls over on a GaN surface. We propose these undamaged regions act as lattice matched patches on a disordered surface and allow the overgrowth of the NWs.

By decreasing the pitch in the spot array to 3.5 nm (beam spot overlap of 50%), both 85 and 262 ions/pulse cause reorientation of the NWs when approaching the disordered regions (Figure 2e–h). In this case, the unexposed diamond-shaped regions on GaN are eliminated and areal distribution of surface disorder becomes more uniform blocking the epitaxial growth of the ZnO in this region.

We also note that by decreasing the spot pitch to 3.5 nm, we are in fact increasing the average ion dose introduced to the exposed surface by a factor of 4 (Figure S5, Supporting Information). Therefore, it is plausible to attribute the blockage of the nanoepitaxy to a higher average ion beam. To determine the contribution of the average ion dose versus the size of the lattice-matched patches (undamaged areas), we used an average ion dose of 267 at 3.5 and 7 nm pitches. This average ion intensity at a 3.5 nm pitch is sufficient to block the nanoepitaxy

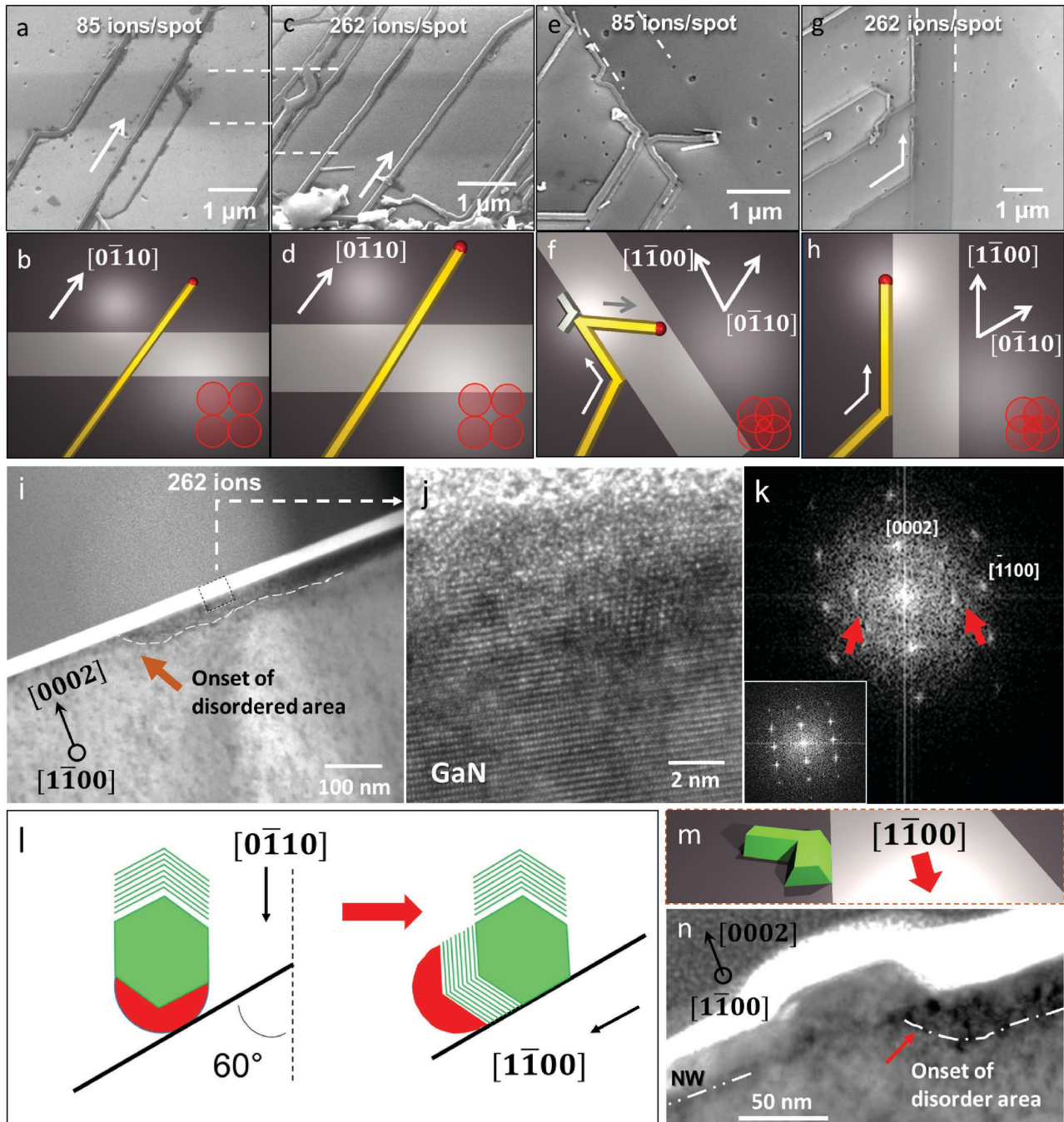


Figure 2. SEM and schematics of nanocrystals encountering disordered GaN areas. These areas are darker stripes seen in (a,c,e,g), approximately 1 μm wide and are regions patterned with a 7 nm ion beam spot. a–d) At zero spot overlap, i.e., 7 nm pitch, nanocrystals navigate through the disordered areas. e–h) At 50% spot overlap, i.e., 3.5 nm pitch, nanocrystal growth vectors rotate to the next available m -direction. i,j) TEM cross-section of a disordered region made at highest dose (262 ions) at a 3.5 nm pitch. Analysis reveals no discernable losses to substrate surface; however, k) shows formation of nanocrystallites of GaN within the disorder region. l) If disorder patterns, at 3.5 nm spot pitch, are drawn at 60° relative to nanocrystal growth vectors, it cause rotations adjacent to the m -direction shifting the Au nanodroplet to the front of the new growth vector. In this scenario m) the nanocrystal starts growing parallel to the disorder pattern. n) Cross-section of the nanocrystal when it encounters the disorder pattern.

(Figure S6, Supporting Information); however, at a 7 nm pitch, we observe a directed nanocrystal epitaxy over the patterned areas (Figure S7, Supporting Information). Overall results indicate that size and spacing of the lattice-matched patches on the substrate are crucial in allowing the lateral nanoepitaxy.

To better understand the blockade of epitaxy and change in nanocrystal direction at a 262 ions/pulse 3.5 nm pitched array, cross-sectional HRTEM of GaN in the disordered regions was carried out. In Figure 2j) the onset of the ion-exposed line pattern is clearly seen with a darker contrast-indicating the

penetration of Ga ions to a depth of about 30 nm. Simulations (Figure S1, Supporting Information) show the greatest population of stopped 30 keV Ga⁺ ions in GaN are ≈14 nm deep, which is significantly less than what we experimentally observe. This discrepancy is attributed to the enhancement due to the channeling effect along the 0001 direction of the GaN lattice,^[20] a feature not considered in the simulation models. Within this penetration range, Ga⁺ ions are expected to frequently stop, generating point defects including interstitial Ga as well as vacancies within the lattice.

Examining the unexposed and exposed GaN surface does not show any surface atom removal due to sputtering; however, HRTEM shows loss of lattice order in the 6 nm region below its surface as shown in Figure 2k. Interestingly, the representative FFT pattern of this region (Figure 2k) shows appearance of a ring pattern for (0001) GaN plane indicating formation of nanocrystalline GaN fragments at the surface with arbitrary *c*-directions. These polycrystalline regions are also expected to exist in the 262 ions/pulse patterns pitched at 7 nm (0% overlap); however, they are surrounded by 4–7 nm size patches of ordered GaN that are few nanometers apart. These ordered areas enable a growing nanocrystal to anchor to and build a single crystal structure as it grows over the disordered region. Of course, in the case of the 50% overlap, the patches of lattice matched regions are negligible and the growing nanocrystal cannot continue its epitaxy. If one of the six *m*-directions of the ZnO nanocrystal is parallel to the edge of the disordered region, it guarantees blockade of that specific crystal facet but growth along an adjacent facet resulting in a 60° rotation in the growth vector.

The change of direction requires migration of the Au droplet to those facets as shown in the schematic of Figure 2m to continue the nanocrystal growth in another *m*-direction while maintaining its original width. The TEM of Figure 2n captures a cross-section of a nanocrystal where it is forced to change its direction to [1 $\bar{1}$ 00]. TEM shows that the laterally growing nanocrystal does not exactly change path at the onset of the surface disorder (Figure 2n, dashed line) and overgrows about 20 nm within the disordered area, most likely due to the reduced density of surface disorder at the edge of the pattern. HRTEM analysis of different parts of the nanocrystal shows that the formed n-ZnO/p-GaN heterojunction remains single crystal with no specific defects in the ZnO over the disordered and ordered GaN regions (Figure S2, Supporting Information).

Interestingly, if the disordered pattern (50% spot overlap) is placed with a 30° offset relative to the *m*-direction of the GaN (or ZnO nanocrystal) as illustrated in Figure 3a, the six-sided nanocrystal touches the disorder pattern from its vertex, switching to another *m*-direction after a 60° reflection. This effect is demonstrated in Figure 3b using disorder patterns made from 262 ions/pulses at 50% overlap. The growth of the nanocrystals in an *m*-direction shows it is primarily the nanocrystal which defines the preferred growth facets and wetting by Au droplet is a secondary factor. Perhaps most strikingly is the response of a nanocrystal within the geometrical boundaries above as illustrated in Figure 3c,d. In this case, the growth vector changes several times much like that of the reflection of a beam of light.

In addition to the lateral control over the morphology of the nanocrystals, it is possible to overgrow a hexagonal nanocrystal such as ZnO in its [0001] direction using a vapor-solid (VS) growth process (during the lateral growth) to form nanowalls with controllable geometries as in Figure 3e,f. Kinked nanowires have been previously shown in free-standing NWs via the VLS process^[21] in which the plane of growth is changed using variation in the gaseous composition of the chamber temperature, etc.; however, the control over yield, reproducibility and scalability have shown to be uncertain and challenging.

By setting proper surface boundaries, the proposed method allows the partitioning of NW heterojunctions into different segments with predictable orientational order in a scalable and predictable fashion. A simple example of this approach in Figure 3g shows the first illustration of filtering laterally grown nanocrystals to individual NWs. To feed the ZnO nanocrystals to the patterned area the Au pattern is positioned at the entrance of the parallel line patterns made by Ga ions (50% spot overlap). Under this condition, multiple NWs could enter a channel; however, only a single NW continues its growth and the rest are terminated after encountering the side barriers. Such control could be of use in applications where long NWs or lateral junctions are needed to be folded to fit into a compact area or in photonic circuits where growth path of nanocrystals and their number must be predictable and different parts of a nanocrystal needs to have different orientations.

As stated above, the 262 ions/pulse irradiation forms polycrystalline GaN in the exposed spots as depicted in Figure 2j,k. When spots are overlapped 50%, the patterned regions block the nanocrystals at their point of entry, regardless of the number of times they hit a pattern (Figure 3). Therefore, it is plausible to consider these regions as epitaxially inaccessible zones. However, we do see an increase in the likelihood of growth over the patterned regions even at a 50% spot overlap as the ion dose is reduced. For instance, by reducing the dose to 1/3 (85 ions/pulse), successful navigation of nanocrystals in the [1010] *m*-direction of GaN takes place, indicative of restoration of an epitaxial relationship between ZnO and GaN. Cross-section of a representative ZnO nanocrystal is shown in Figure 4a–c. HRTEM (Figure 4b) and scanning transmission electron microscopy (STEM) analyses show the ZnO crystal grown over the disordered region has a high quality structure with no detectable defects. Examination of the ZnO/GaN interface (Figure 4c) and inset FFT pattern show a coherent epitaxy at the interface that can also be deduced from the STEM results (Figure S3, Supporting Information). No high order defects such as misfit dislocations or stacking faults are observed in the examined cross-sections both in STEM and TEM modes, although their formation as well as local lattice strain cannot be ruled out. Overall results suggest that the surface disordered regions could undergo a structural reformation during high temperature reaction conditions, which becomes more effective as the ion dose is reduced.

For lower doses such as 9 ions/pulse, the extent of structural disorder is insignificant; however, it is enough to change the electronic structure of the heterojunction at the interface as observed by CL microscopy. Representative SEM image in Figure 4d shows several NWs grown over the ion-patterned area

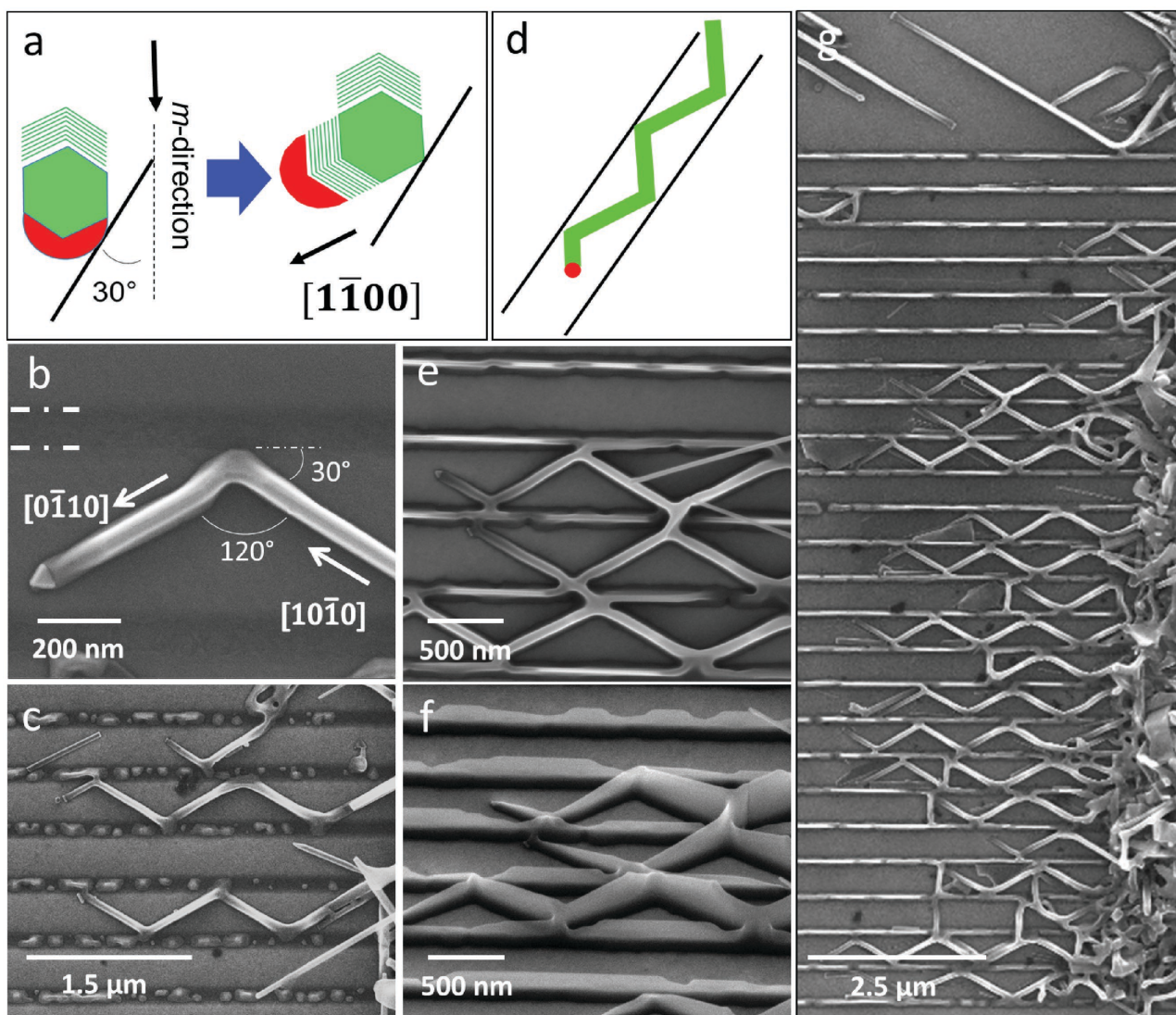


Figure 3. a,b) Disorder line pattern (262 ions, 3.5 nm pitch) positioned 30° relative to initial nanocrystal growth vector causes rotation to next available *m*-direction. c,d) Linear geometrical boundaries of 100 nm wide patterns confine growing nanocrystals to a narrow channel, “reflecting” the NW back and forth. e,f) Disorder patterns provide nucleation zones for VS growth of ZnO nanowalls. g) Guiding ZnO NWs to parallel line patterns confines their growth and filters out NWs illustrating simultaneous control over their orientation and number.

(dashed lines) and Figure 4e illustrates their corresponding CL image.

ZnO NWs are seen to glow brightly in both Areas 1 and 2 of the CL image indicating the majority of radiative e-h recombination takes place within the ZnO side. The dark band (Area 2) in Figure 4e indicates weaker emission of GaN corresponding to the ion-exposed region of the substrate. Spatially resolved CL spectra of the heterojunctions in both areas were obtained using line scans along their length (red and green dots) and were averaged together as in Figure 4g. The CL spectrum (black curve, Area 1) shows the near-band edge emission of n-ZnO NWs/p-GaN is at about 372 nm, indicating a 13 nm blueshift relative to the known 385 nm emission of free-standing ZnO NWs or bulk ZnO.^[22] The lower energy peak at 430 nm in the CL spectrum is a characteristic peak of p-GaN and has been attributed to the transitions from the conduction band or

shallow donors to the Mg acceptor levels (donor-acceptor).^[23] The same figure shows the CL spectra corresponding to the emission of the segment of the heterojunctions grown over the ion exposed region (orange curve, Area 2). Compared to Area 1, we observe a loss in the intensity of the ZnO 372 nm peak within the ion exposed region. However, a rise in intensity is observed in other specimens. A comprehensive survey of NW heterojunctions shows that this variation is not due to crystal defects but rather arises from the thickness variation of the nanocrystal along its length, which in turn impacts the ZnO volume excited by high energy electrons (Figure S4, Supporting Information.^[24] Comparing Areas 1 and 2 also shows a considerable decrease in the emission intensity of the GaN:Mg substrate at 430 nm within Area 2.

Simulation (Figure 4g) shows when the 5 keV electron beam is focused on a NW with a typical height of about 30 nm, the

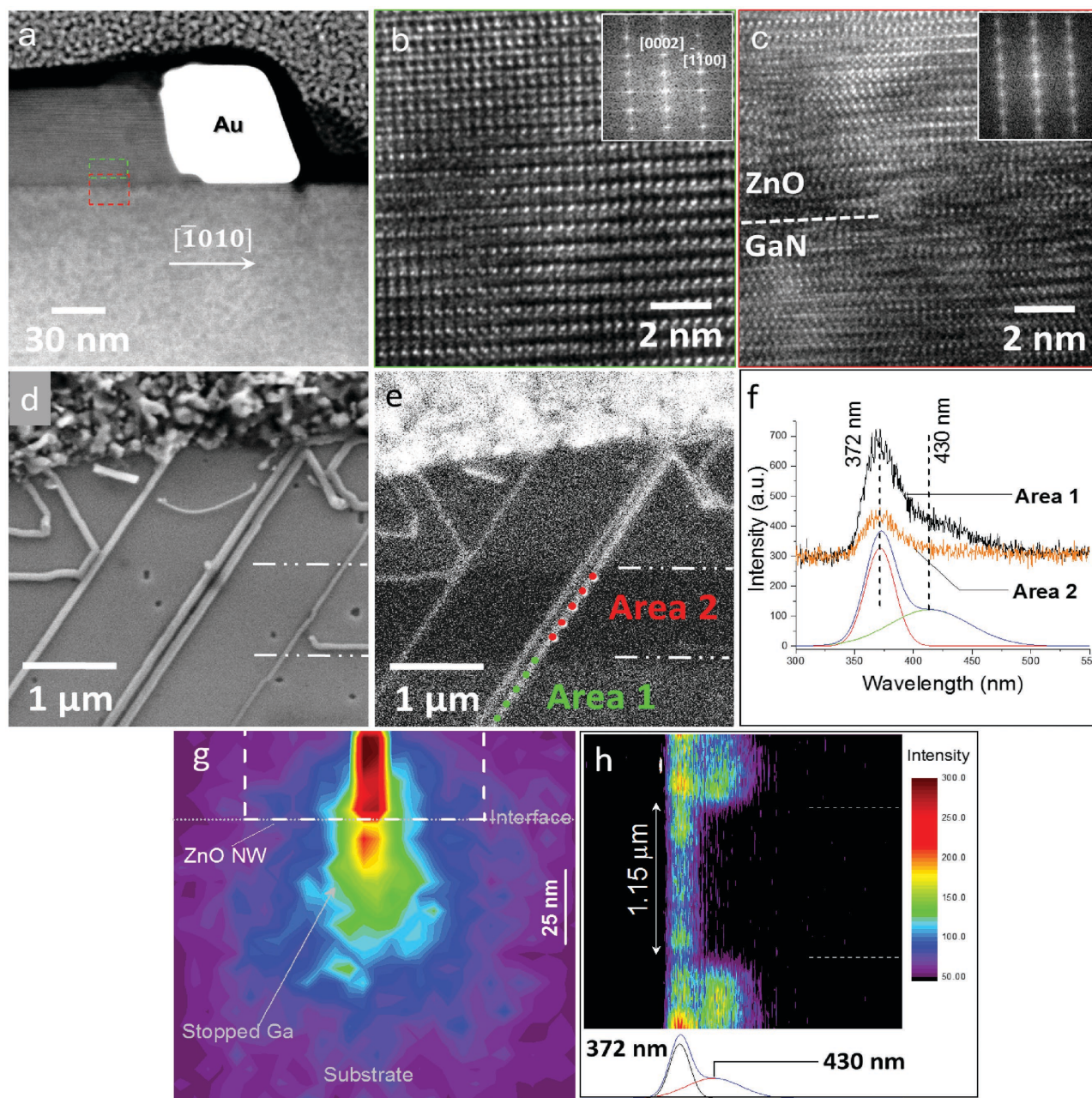


Figure 4. a) Dark field STEM image of a ZnO nanocrystal/Au grown over GaN patterned with a 3.5 nm pitch array of disorder (85 ions/pulse). HRTEM of b) ZnO lattice immediately above interface and c) interface between ZnO and GaN lattices reveals restoration of nanoepitaxy between crystals and no discernable occurrence of crystal defects. d,e) SEM and CL images of NWs grown over disorder regions (area 2) patterned with 9 ions/pulse at 7 nm pitch). f) Averaged spectra from area 2 and area 1 (NW over pristine GaN) show donor–acceptor recombination peak is lost in Area 2; g) Energy loss mapping of 5 keV electron beam used to survey NWs indicates the excitation volume is mainly with the NW and at the interface. h) Full CL line scan rendered as a map of wavelength signal intensity versus linear position on NW illustrates the abrupt onset of disorder region where 430 nm signal is lost and resumes outside of the region.

majority of the energy loss is concentrated in a volume of about 13 nm in radius and about 95 nm deep most of which falls within the volume of the NW with some of the lower energy electrons (roughly between 2.5 and 1.25 keV) reaching to about 30 nm below the interface. Therefore, most of the observed CL signal originates from the ZnO nanocrystal and part from the immediate underlying substrate resulting in a weak 430 nm

peak. The suppression of this peak in the heterojunctions of Area 2 is attributed to the loss of Mg acceptor levels of the *p*-GaN most likely due to their displacement in lattice. The formed vacancies or interstitials clearly did not create a significant population of deep-trap states both in ZnO and GaN as evident by the undetectable emissions at 550–560 nm.^[25] Figure 4h depicts a full line emission scan (250–650 nm

spectrum) along the length of a single NW rendered as an image highlighting the spatial variation of the 372 and 430 nm peaks across the NW over the disordered region. If the *p*-type nature of GaN is represented by the 430 nm peak, this image clearly shows the disappearance of the *p*-nature of the substrate in Area 2 and an example for local change in doping profile along a 2D heterojunction without observable changes to the crystal structure or morphology of the overgrown nanocrystal. These results indicate that varying crystal structure or composition within few nanometers of the surface could be used as an effective tool for modulating the growth habits and properties of surface-directed nanocrystals.

In summary we report, to the best of our knowledge, the first examples of concerted response of laterally grown nanocrystals to local variation in surface lattice disorder in terms of their dynamics, crystal structure and optical characteristics. SVLS-grown nanocrystals were used as in situ nanoprobe to gauge the significance of the substrate disorder on epitaxial nanocrystal growth. For a highly lattice matched system such as ZnO/GaN, we reduced the lattice match to block the epitaxy and then increased the match by creating lattice matched zones on GaN. These zones were formed using a tightly focused ion beam to ensure they remain smaller compared to the overgrown nanocrystal. The presence of an approximate 20% GaN surface unit cells was found to be necessary to allow the epitaxial overgrowth of a nanocrystal. At or above this threshold, nanoepitaxy occurs and the electronic states of the substrate surface could be spatially changed without changing the nanocrystal's direction or optical characteristics. Below this threshold, i.e., by reducing the lattice matched zones, nanoepitaxy stops. This property was used to demonstrate a novel approach for guiding laterally grown nanocrystals using local surface boundaries to partition NW heterojunctions into different segments and orientations as well as filtering their numbers. The observed threshold highlights the remarkable tolerance of crawling nanocrystals to strain and lattice mismatch and prospect of realization of exotic combinations of nanocrystals, e.g., nanoepitaxy over surfaces decorated with patches of 2D inorganic islands. Addition of such capabilities to the surface-directed VLS growth method is expected to enable spatially controlled-alteration of the electronic structure, doping profile or morphology of laterally grown nanocrystals and will further its dexterity in realization of highly ordered heterogeneous nanosystems.

Experimental Section

The SVLS process used to grow ZnO nanocrystals and NWs was carried out in a horizontal tube furnace with 800 mm length and 49 mm inner diameter. A ZnO/Graphite mixture of 0.140 g (1:1 mass ratio) was positioned at the center of a small quartz tube with a 130 mm length and 19 mm inner diameter. The tube furnace temperature was at 890 °C (with a ramp rate of ≈ 111 °C min⁻¹) and a dwell time of 40 min under ≈ 0.5 standard liters per minute (SLPM) flow of ultra-dry (99.99%) N₂ gas. NWs were grown on a 2 μ m thick *c* plane NOVAGAN^[26] GaN (on *c* plane sapphire) doped with Mg to a concentration of 5×10^{17} atoms cm⁻³. Gold patterns were deposited using a thermal evaporator.

Doses of ions per pulse were controlled by monitoring beam current and adjusting pulse time, resulting in average doses of (9, 26, 85, and 262) ions/pulse/spot at ≈ 4 pA of current within 7 nm diameter spots. Note that these values are average number of ions per pulse, since the

ions are Poisson distributed. Furthermore, at the lowest doses, there is a $\pm 30\%$ variation in the number of ions per spot, however, over the large patterned areas this variation is expected to be averaged out. For these patterns, the ion beam was focused on a ZnO nanoparticle targets and spot size was checked using knife-edge protocols implemented in the "Image" (v1.05.00 build 020) code developed by FEI, which closely follows ISO established method: ISO TC 202/SC4. Simulations of Ga⁺ ion trajectory, stopping range, and displacement probabilities were performed using the SRIM code which leverages the binary collision approximation to predict ion scattering behavior and material modification. Monolayer collision steps of 30 keV Ga⁺ ions at 0° incident angles with respect to the normal direction of the target GaN surface, with collision details, sputtered atoms, and ion ranges tracked. Detailed information on simulations of sputtering can be found in Figure S1 in the Supporting Information.^[27–30]

SEM measurements were carried out using 20 keV electrons with a nominal spots size of about 1 nm. CL measurements were performed using an FEI Quanta 200 outfitted with a Gatan Elite series Mono4CL. CL acquisition parameters were set to 5 keV electron beams with nominal beam spot of ≈ 2 nm diameter and a current of about 0.1 nA. Working distances were optimized for each measurement (between 11.06 and 11.16 mm) to maximize signal to noise with the photomultiplier tube set to -602 V. All spectra were obtained at room temperature (RT) at chamber pressures between 4×10^{-4} and 7×10^{-5} Pa. TEM images were captured using an FEI Titan 80–300 TEM/STEM with a 300 keV electron beam through nominal sample thicknesses of ≈ 120 nm. Lattice images in TEM mode were acquired through a 60 μ m objective aperture using a BM Ultrascan 1000FT CCD camera for an exposure time of 1 s. Fourier transforms of each image were calculated using the Gatan Digital Micrograph software (v1.93).

Supporting Information

Supporting Information is available from the Wiley Online Library or from the author.

Acknowledgements

The authors would like to thank Dr. Andrew Herzing for the many useful discussions about instrumentation and analysis of data.

Received: September 29, 2015

Revised: November 21, 2015

Published online:

- [1] a) N. A. Melosh, A. Boukai, F. Diana, B. Gerardot, A. Badolato, P. M. Petroff, J. R. Heath, *Science* **2003**, *300*, 112; b) A. Javey, Nam, R. S. Friedman, H. Yan, C. M. Lieber, *Nano Lett.* **2007**, *7*, 773; c) S. Xu, Y. Ding, Y. Wei, H. Fang, Y. Shen, A. K. Sood, D. L. Polla, Z. L. Wang, *J. Am. Chem. Soc.* **2009**, *131*, 6670; d) A. Pevzner, Y. Engel, R. Elnathan, T. Ducobni, M. Ben-Ishai, K. Reddy, N. Shpaisman, A. Tsukernik, M. Oksman, F. Patolsky, *Nano Lett.* **2010**, *10*, 1202; e) E. Saeedi, C. Marcheselli, A. Shum, B. A. Parviz, *Nanotechnology* **2010**, *21*, 375604.
- [2] A. Yu Cao, C. M. Lieber, *Nat. Nano* **2007**, *2*, 372.
- [3] A. Cunningham, *Explorer, Nanoelectronics*, Strategic Business Insights, Menlo Park, CA, **2014**.
- [4] a) M. A. Meitl, Z.-T. Zhu, V. Kumar, K. J. Lee, X. Feng, Y. Y. Huang, I. Adesida, R. G. Nuzzo, J. A. Rogers, *Nat. Mater* **2006**, *5*, 33; b) R. Yerushalmi, Z. A. Jacobson, J. C. Ho, Z. Fan, A. Javey, *Appl. Phys. Lett.* **2007**, *91*, 203104.
- [5] K. Takei, T. Takahashi, J. C. Ho, H. Ko, A. G. Gillies, P. W. Leu, R. S. Fearing, A. Javey, *Nat. Mater* **2010**, *9*, 821.

- [6] Z. Fan, J. C. Ho, Z. A. Jacobson, H. Razavi, A. Javey, *Proc. Natl. Acad. Sci.* **2008**, *105*, 11066.
- [7] B. Nikoobakht, C. A. Michaels, S. J. Stranick, M. D. Vaudin, *Appl. Phys. Lett.* **2004**, *85*, 3244.
- [8] B. Nikoobakht, A. Herzing, *ACS Nano* **2010**, *4*, 5877.
- [9] M. Schwartzman, D. Tsivion, D. Mahalu, O. Raslin, E. Joselevich, *Proc. Natl. Acad. Sci.* **2013**, *110*, 15195.
- [10] S. A. Fortuna, J. Wen, I. S. Chun, X. Li, *Nano Lett.* **2008**, *8*, 4421.
- [11] J. Y. Lao, J. Y. Huang, D. Z. Wang, Z. F. Ren, *Adv. Mater.* **2004**, *16*, 65.
- [12] Y. Shen, S. Turner, P. Yang, G. Van Tendeloo, O. I. Lebedev, T. Wu, *Nano Lett.* **2014**, *14*, 4342.
- [13] Z. Wu, M. G. Hahm, Y. J. Jung, L. Menon, *J. Mater. Chem.* **2009**, *19*, 463.
- [14] Z. Zhang, L. M. Wong, H. X. Wang, Z. P. Wei, W. Zhou, S. J. Wang, T. Wu, *Adv. Funct. Mater.* **2010**, *20*, 2511.
- [15] E. Oksenberg, R. Popovitz-Biro, K. Rechav, E. Joselevich, *Adv. Mater.* **2015**, *27*, 3973.
- [16] R. D. Robinson, B. Sadtler, D. O. Demchenko, C. K. Erdonmez, L.-W. Wang, A. P. Alivisatos, *Science* **2007**, *317*, 355.
- [17] J. C. Ho, R. Yerushalmi, Z. A. Jacobson, Z. Fan, R. L. Alley, A. Javey, *Nat Mater.* **2008**, *7*, 62.
- [18] B. Nikoobakht, J. Bonevich, A. Herzing, *J. Phys. Chem. C* **2011**, *115*, 9961.
- [19] J. F. Ziegler, M. D. Ziegler, J. P. Biersack, *Nucl. Instrum. Methods Phys. Res., Sect. B* **2010**, *268*, 1818.
- [20] E. V. Kornelsen, F. Brown, J. A. Davies, B. Domeij, G. R. Piercy, *Phys. Rev.* **1964**, *136*, A849.
- [21] B. Tian, P. Xie, T. J. Kempa, D. C. Bell, C. M. Lieber, *Nat. Nano* **2009**, *4*, 824.
- [22] a) H. J. Fan, R. Scholz, M. Zacharias, U. Gösele, F. Bertram, D. Forster, J. Christen, *Appl. Phys. Lett.* **2005**, *86*, 023113; b) M. Lorenz, J. Lenzner, E. M. Kaidashev, H. Hochmuth, M. Grundmann, *Ann. Der Physik* **2004**, *13*, 39; c) B. S. Li, Y. C. Liu, Z. S. Chu, D. Z. Shen, Y. M. Lu, J. Y. Zhang, X. W. Fan, *J. Appl. Phys.* **2002**, *91*, 501.
- [23] a) S. Nakamura, T. Mukai, M. Senoh, *Jpn. J. Appl. Phys.* **1991**, *30*, L1998; b) U. Kaufmann, M. Kunzer, M. Maier, H. Oblo, A. Ramakrishnan, B. Santic, P. Schlotter, *Appl. Phys. Lett.* **1998**, *72*, 1326; c) K. H. B. H. Obloh, U. Kaufmann, M. Kunzer, M. Maier, A. Ramakrishnan, P. Schlotter, *J. Cryst. Growth* **1998**, *195*, 270.
- [24] K. Pearson, *Proc. R. Soc. Lond.* **1895**, *58*, 240.
- [25] X. Li, P. W. Bohn, J. J. Coleman, *Appl. Phys. Lett.* **1999**, *75*, 4049.
- [26] Certain commercial equipment, instruments, materials, or software are identified in this paper to foster understanding. Such identification does not imply recommendation or endorsement by the National Institute of Standards and Technology, nor does it imply that the materials or equipment identified are necessarily the best available for the purpose.
- [27] J. Neugebauer, *Nitride Semiconductors*, Wiley-VCH, Weinheim, Germany, **2006**, p. 295.
- [28] A. Y. Polyakov, S. J. Pearton, P. Frenzer, F. Ren, L. Liu, J. Kim, *J. Mater. Chem. C* **2013**, *1*, 877.
- [29] J. P. Biersack, W. Eckstein, *Appl. Phys. A* **1984**, *34*, 73.
- [30] a) I. Chyr, A. J. Steckl, *J. Vac. Sci. Technol. B* **2001**, *19*, 2547; b) A. J. Steckl, I. Chyr, *J. Vac. Sci. Technol. B* **1999**, *17*, 362.